

Effect of zinc content on structural, functional, morphological, and thermal properties of kappa-carrageenan/NaCMC nanocomposites

Farzaneh Sabbagh^a, Khadijeh Kiarostami^{a,*}, Nadia Mahmoudi Khatir^b, Shahabaldin Rezaia^{c,**}, Ida Idayu Muhamad^d, Fakhrisadat Hosseini^b

^a Department of Plant Sciences, Faculty of Biological Science, Alzahra University, 1993891176, Tehran, Iran

^b Department of Biotechnology, Faculty of Biological Science, Alzahra University, 1993891176, Tehran, Iran

^c Department of Environment and Energy, Sejong University, Seoul, 05006, South Korea

^d Department of Bioprocess & Polymer Engineering, Faculty of Engineering, Universiti Teknologi Malaysia, 81310, Johor, Malaysia

ARTICLE INFO

Keywords:

Doping concentration
MgO composite
Nanocomposite materials
Carrageenan gel
Sol-gel synthesis

ABSTRACT

This study was aimed to produce a novel nanocomposite with appropriate properties to apply in biomedical researches. MgO was used as a control sample in the experiments. A series of $Mg_{1-x}Zn_xO$ nanoparticles with $x = 0.01$ and 0.03 , were prepared by the sol-gel method and added to k-carrageenan/NaCMC to produce MgO , $Mg_{0.99}Zn_{0.01}O$, and $Mg_{0.97}Zn_{0.03}O$ /k-carrageenan/NaCMC hydrogels. The structural properties were systematically investigated using X-ray diffraction (XRD), Swelling ratio %, Fourier-transform infrared spectroscopy (FTIR), Field Emission Scanning Electron Microscope (FESEM), Thermal Gravimetric Analysis (TGA), and Compression test. The FESEM analysis showed that the doping of 'Zn' in MgO had a strong effect on morphology and crystallinity of MgO nanoparticles. The MgO nanocomposite had the lowest swelling ratio. The swelling started to increase at $3.37 \pm 0.95\%$ and was found to finish at $3.81 \pm 0.26\%$, including a peak at $22.1 \pm 6.76\%$ in the graph. The highest swelling ratio was attributed to $Mg_{0.99}Zn_{0.01}O$ with the final ratio of $44.15 \pm 1.98\%$. The TGA analysis revealed that total weight loss of MgO nanocomposite was greater than $Mg_{0.99}Zn_{0.01}O$, and $Mg_{0.97}Zn_{0.03}O$. The compression test of the nanocomposites showed that the hardness of MgO nanocomposite was the highest and it was 89.75 ± 9.19 (g), the springiness of $Mg_{0.99}Zn_{0.01}O$ and $Mg_{0.97}Zn_{0.03}O$ was the same and it was 10 (mm), the adhesion of $Mg_{0.97}Zn_{0.03}O$ showed -0.848 ± 0.29 that was highest, however the consistency of $Mg_{0.99}Zn_{0.01}O$ showed 392.90 ± 3.48 (g. sec).

1. Introduction

Bio nanocomposites are a combination of inorganic materials and biopolymers, mostly metals such as SiO_2 , silver, TiO_2 , and ZnO in nano-dimensions [1]. Some of their characteristics include high thermal resistance, high mechanical strength, and low permeability against water vapor and gases [2]. The reason to select ZnO among different nanoparticles ZnO is its environment-friendly, antibacterial, non-toxic, inexpensive, and without harmful impacts on the body cells [3]. The doping of Mg into ZnO particles could improve their preferential orientation growth [4]. Usually, high heat treatment temperature leads to large crystallite size and good preferential orientation meanwhile, a low temperature favors small crystallite size [5].

Among inorganic materials, metal oxides such as MgO are stable under harsh process conditions and are known to be essential minerals for human health [6]. MgO nanoparticles are well known for their biological applications which are beneficial depending on its size, composition, concentration, exposure time and nature of the biological properties. MgO indexed as one of the six magnesium compounds which are currently recognized as safe by the U. S [7] and Food and Drug Administration (21CFR184.1431) [8]. The results indicated that the low concentration of MgO nanoparticles (below 200 g/ml) exhibited non-cytotoxicity. However, once the concentration of MgO nanoparticles was higher than 500 g/ml, the relative growth rate was lower than the control [9].

Among biopolymers, kappa-carrageenan is available naturally which

* Corresponding author.

** Corresponding author.

E-mail addresses: f.sabbagh@alzahra.ac.ir (F. Sabbagh), Kh.kiarostami@alzahra.ac.ir (K. Kiarostami), n.khatir@alzahra.ac.ir (N.M. Khatir), Shahab.rezaia@sejong.ac.kr (S. Rezaia), idaidayu@utm.my (I.I. Muhamad), f.hosseini@alzahra.ac.ir (F. Hosseini).

<https://doi.org/10.1016/j.polymeresting.2020.106922>

Received 23 May 2020; Received in revised form 1 August 2020; Accepted 18 October 2020

Available online 22 October 2020

0142-9418/© 2020 Published by Elsevier Ltd. This is an open access article under the CC BY-NC-ND license (<http://creativecommons.org/licenses/by-nc-nd/4.0/>).

Table 1
Calculation to prepare 2 gr Nanoparticle.

Sample	Mg (NO ₃) ₂ .6H ₂ O (g)	Zn (NO ₃) ₂ .6H ₂ O (g)
MgZnO nanoparticles	12.72488	0
Mg _{0.99} Zn _{0.01} O nanoparticles	12.67406	0.148537
Mg _{0.97} Zn _{0.03} O nanoparticles	12.57053	0.451084

can be isolated from marine red algae [10]. According to the position and number of sulfate groups in the repeating units, carrageenans can be divided into alpha, lambda, iota, kappa, theta and beta [11]. The major gel-forming fractions of polysaccharide are iota- and kappa-carrageenan [12]. The hydroxyl groups of these monosaccharides can be substituted, sulfated, and methylated by D-xyloresidues or pyruvic acid [13]. Particularly, it can easily cross-link ionically with some ions, such as calcium (Ca²⁺) and potassium (K⁺) [14]. Owing to their unique physicochemical properties, carrageenan is widely used in the food industry as stabilizers, thickeners, and emulsifiers [15], in biotechnology and in cosmetology [16]. Carrageenan have an expansive spectrum of biological interest: antiviral [17], antitumor [18], and immunomodulating [19], antioxidant [20]. Since polymers need to have appropriate water absorption (swelling) and mechanical characteristics, a combination of κ -Carrageenan, NaCMC, and different levels of MgZnO has been used to produce hydrogels [21].

In this study, undoped and Zn-doped MgO nanostructures grown by using a sol-gel method in a gel media to obtain the morphology for the undoped and Zn- doped MgO nanostructures. Then, Zn co-doped MgO films have been fabricated by the sol-gel process and effects of the doping on the structural. In addition, the morphological properties of the films have been investigated and the effects of nanoparticle ratios of fabricated hydrogels as an important processing factor on key properties of a hydrogel were evaluated. Although the loading of catechin in hydrogel samples that were produced by the physical method will be conducted and evaluated as well, and the influence of nanoparticles on the release rate of catechin will be characterized and will be reported in the next paper. Finally, thermal and mechanical properties were investigated in optimum formulations.

2. Materials and methods

2.1. Materials

In this study calcium carbonate (CaCO₃), κ -Carrageenan, Magnesium nitrate hexahydrate, sodium carboxymethyl cellulose (NaCMC), (+)-Catechin hydrate, Zinc nitrate hexahydrate, and gelatin (an agent for polymerization and stabilization) were all attained from Sigma-Aldrich (Missouri-USA) and applied without any additional purification. Distilled water was applied in the synthesis of the hydrogel.

2.2. Particles preparation and characterization

To prepare the Zn-doped MgO nanoparticles in the form of Mg_{1-x}Zn_xO, where x = 0, 0.01 and 0.03 the analytical grade of Zinc nitrate hexahydrate (Zn(NO₃)₂.6H₂O), Magnesium nitrate hexahydrate (Mg(NO₃)₂.6H₂O), gelatin [(NHCOCH-R)_n, R1 = amino acid, Type A, Porsin], and distilled water are used. To prepare the amount of 2 g nanoparticles, Mg and Zn nitrates were dissolved in 20 ml of distilled water (Table 1).

The rate of the nitrates was calculated due to the Mg_{1-x}Zn_xO formula, where x = 0.01 and 0.03. By preference, 4 g of gelatin (the scale of final product to the gelatin was 1:2) dissolved in 60 ml of distilled water, and using an oil bath, the solution was stirred at 80 °C constantly. Then, the solution of Mg²⁺ and Zn²⁺ was mixed with the solution of gelatin. By stirring for 7 h at a constant temperature of 80 °C continuously, a viscous, transparent, and honey-like gel was obtained. A modicum of the prepared gel inserted into the kiln for the calcination process with the

operation temperature of 600 °C and duration of 2 h with a heating rate of 5 °C/min [22].

2.3. Preparation of κ – carrageenan/NaCMC and metal nanocomposites hydrogel

For hydrogel fabrication, 0.12 g NaCMC, and 0.48 g of κ -carrageenan was thawed in 20 ml of distilled water at 80 °C and 0.15 g CaCO₃ dissolved in 10 ml distilled water separately. The mix of both solutions was stirred for 1 h until a viscous, clear and homogenous solution was obtained without any bubble [23]. Then, 0.8 mg/ml aqueous solution of Mg_{0.99}Zn_{0.01}O, Mg_{0.97}Zn_{0.03}O and MgO was prepared. Then, the aqueous solution of Mg_{0.99}Zn_{0.01}O, Mg_{0.97}Zn_{0.03}O, and MgO each was added to κ -Carrageenan/NaCMC solution and stirred at room temperature until the hydrogels were formed [24].

2.4. X-ray diffraction (XRD) analysis

XRD analysis was performed by powder diffractometer (SEIFERT PTS 3003, Rigaku, Ultima IV, Japan) which was attached with a Cu K α radiation (λ = 1.54 Å) [25].

2.5. Morphology of nanoparticles and nanocomposite hydrogels

To study the FESEM, gold-coated nanoparticles were mounted under vacuum, on a holder, and then gaged into a LEO 1450 V P (20 kV, Ramsey, New Jersey, USA) [23].

2.6. Measuring the swelling ratio of nanocomposite hydrogels

The swelling of the hydrogels was evaluated for 2.0 g of the nanocomposites at ambient temperature and pH 7 besides was calculated using equation (1):

$$\text{Swelling ratio\%} = \frac{W_s - W_0}{W_0} \times 100 \quad (1)$$

where W₀ and W_s are the initial weight of hydrogels and weight of swollen hydrogel at time *t* respectively [26].

2.7. FTIR

Operating an FTIR (Thermo Nicolet Avatar 370, BioSurplus, USA) and potassium bromide coming with wavelength of 4000–400 cm⁻¹, the FTIR spectra was recorded [27].

2.8. Thermogravimetric analysis (TGA)

Operating a Shimadzu apparatus TGA-50(Shimadzu, Japan) all the nanocomposites with the range of 4–8 mg, were heated under nitrogen flow (20 ml/min) and in the range of 30–800 °C at the heating rate of 10 °C/min [28].

2.9. Compression test

A texture analyser (TA. XT. Plus, Stable Micro Systems, UK) was used to measure the consistency, hardness, springiness, and adhesion of the hydrogels. The analytical probe P/0.4 (4 mm diameter, stainless steel cylinder) was condensed within the hydrogels (20 mm height) at a speed of 1.0 mm/s, to a 60% height of sample depth, and with a trigger force of 3 g triplicate [29].

2.10. Statistical analysis

All formulations were expressed as mean \pm standard deviation triplicate. To define a statistically significant difference between

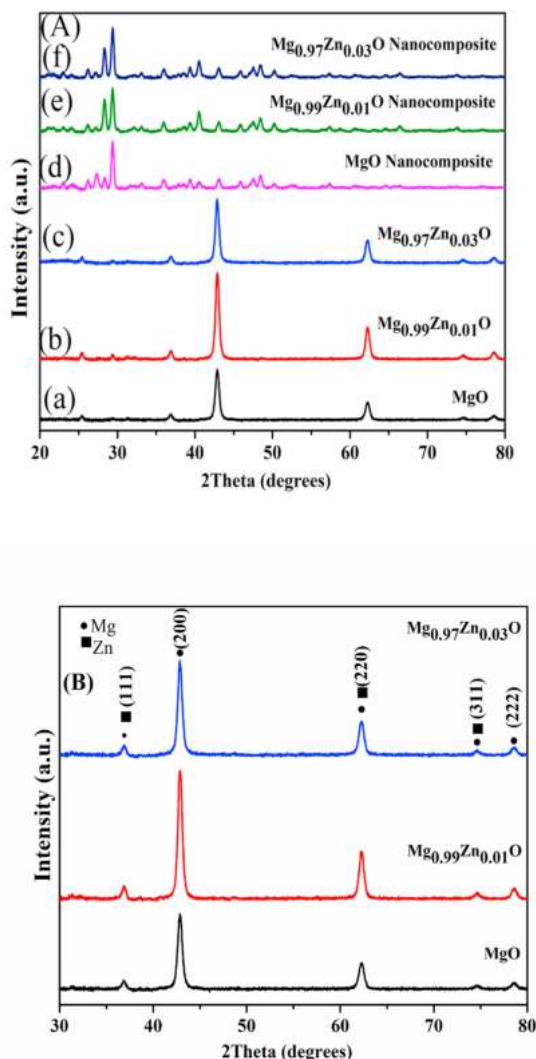


Fig. 1. (A), (B). XRD diffraction patterns of (a) MgO, (b) Mg_{0.99}Zn_{0.01}O, (c) Mg_{0.97}Zn_{0.03}O, (d) MgO nanocomposite, (e) Mg_{0.99}Zn_{0.01}O nanocomposite, and (f) Mg_{0.97}Zn_{0.03}O nanocomposite.

samples, a one-way analysis of variance (ANOVA) with the post “Tukey’s post hoc test” for multiple comparisons was conducted using SPSS software (SPSS, version 18). A *p*-value of less than 0.05 was considered statistically significant.

3. Results and discussion

3.1. XRD patterns of nanoparticle and nanocomposite hydrogels

Fig. 1 shows the crystallinity patterns of Mg_{0.99}Zn_{0.01}O, Mg_{0.97}Zn_{0.03}O and MgO nanoparticle and nanocomposite hydrogels. In the current research, Zn-doped MgO nanoparticles with rate of 0.01 and 0.03 have been used. According to our previous research, we don’t use simple one of them because the intense and sharp peaks indicate the high crystalline in the samples more than simple MgO or ZnO nanoparticles [30]. The crystalline property of κ-Carrageenan/NaCMC hydrogel, Mg_{1-x}Zn_xO nanoparticle was performed by XRD analysis where *x* = 0, 0.01 and 0.03 and κ-Carrageenan/NaCMC/Mg_{1-x}Zn_xO/Catechin hydrogel (Fig. 1). The results revealed that the ZnO hexagonal structure and MgO cubic structure were produced at 650 °C (calcination temperature). Hence, after addition of catechin to the compound, some different diffraction peaks were detected in the patterns. These peaks were indexed to the hexagonal crystalline structure

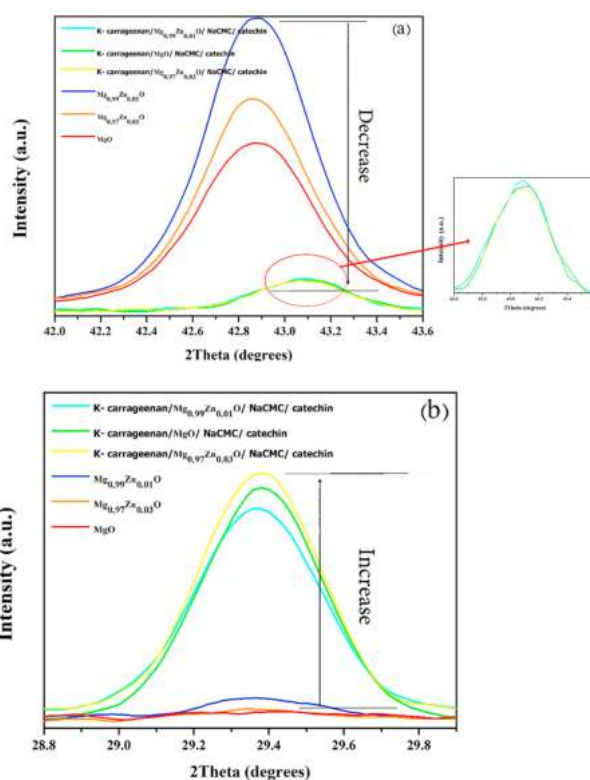


Fig. 2. XRD peak related to (a) MgO cubic (b) ZnO hexagonal structures.

and were appeared at $2\theta = 29, 35, 43$ and 47° . In other words, most ZnO atoms were formed as ZnO nanostructures as well as the MgO-nanoparticles and defused in the cubic structures of ZnO nanoparticles.

Fig. 2(a and b) shows the diffraction peaks related to MgO-nanoparticles and nanocomposite that are associated with the cubic structure of MgO nanoparticle and hexagonal nanocrystals of ZnO, respectively. Fig. 2(a) presents the intensity of the diffraction peaks was decreased as the compound was loaded with impure Mg atoms due to the arisen defects in the cubic structure.

Unsurprisingly, the diffraction peak intensity in Fig. 2(b) increased by increasing the ZnO amount in the compound. The pattern of XRD for κ-Carrageenan/NaCMC hydrogel exhibited many broad diffraction peaks at 30° , suggesting that it had amorphous effects [22,28,31]. The addition of Mg_{0.99}Zn_{0.01}O and Mg_{0.97}Zn_{0.03}O nanoparticle to the κ-Carrageenan/NaCMC hydrogel had no impact on the XRD pattern of the hydrogel extremely, indicating suitable compatibility between κ-Carrageenan/NaCMC and Mg_{0.99}Zn_{0.01}O nanoparticle. Such outcome was in agreement with the results of Liu et al. [32]. They fabricated PFE/κ-Carrageenan (polyphenol-rich pomegranate flesh extract) and PPE/κ-Carrageenan (pomegranate peel extract) films. Existence of PFE and PPE to κ-Carrageenan, did not change the XRD patterns unusually [33].

To calculate the crystalline size, the size-strain plot (SSP) method was chosen. The estimated crystalline sizes for Mg_{0.99}Zn_{0.01}O nanoparticles, Mg_{0.97}Zn_{0.03}O nanoparticles, Mg_{0.99}Zn_{0.01}O nanocomposite and Mg_{0.97}Zn_{0.03}O nanocomposite were 18, 13, 20 and 19 nm respectively. The taken XRD data were considered by the SSP method. In SSP method, using equation (2) $(d_{hkl}\beta_{hkl} \cos\theta)^2$ is plotted regarding $(d_{hkl}^2\beta_{hkl} \cos\theta)$:

$$(d_{hkl}\beta_{hkl} \cos\theta)^2 = \frac{A}{D} (d_{hkl}^2\beta_{hkl} \cos\theta) + \left(\frac{\epsilon}{2}\right)^2 \quad (2)$$

where *D* is the crystalline size, *A* is the plane distance and a constant equal to $\frac{3}{4}$, θ is the peak position, β is the full peak width at half

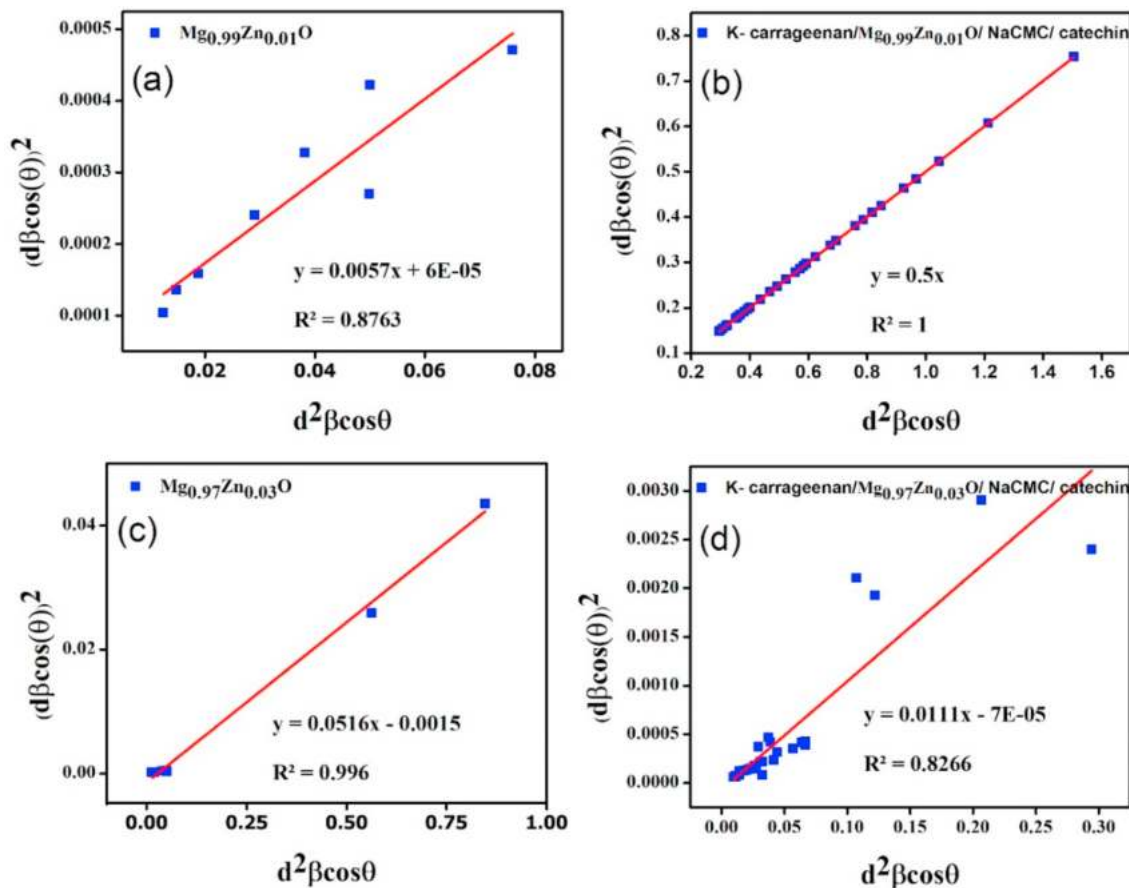


Fig. 3. SSP plot for (a) Mg_{0.99}Zn_{0.01}O nanoparticles, (b) Mg_{0.99}Zn_{0.01}O nanocomposite, (c) Mg_{0.97}Zn_{0.03}O nanoparticles, (d) Mg_{0.97}Zn_{0.03}O nanocomposite.

minimum intensity (FWHM), and ϵ is the lattice strain. The crystalline size of the nanoparticles was valued from the slope of the fitted data. Fig. 3 represents the SSP plots for the samples.

The lattice parameters are calculated by using Bragg equation $\lambda = 2d \sin \theta$ [where d is the distance between two planes with the miller indices (hkl)]. The other parameters are obtained from the lattice geometry equation for cubic structure [34] given by equations (3)–(5):

$$\frac{1}{d^2} = \frac{h^2 + k^2 + l^2}{a^2} \tag{3}$$

$$V = a^3 \tag{4}$$

$$\cos \phi = \frac{h_1 h_2 + k_1 k_2 + l_1 l_2}{\sqrt{(h_1^2 + k_1^2 + l_1^2)(h_2^2 + k_2^2 + l_2^2)}} \tag{5}$$

where Angle ϕ is between planes $(h_1 k_1 l_1)$ and $(h_2 k_2 l_2)$, the broadened XRD peaks then give dislocation density through below equations, which is referred to as the Williamson–Hall (WH) method. The XRD peak width, δ , is related to the strain through the Williamson–Hall (WH)

equation (6) and (7), as below [35]:

$$\delta \frac{\cos \theta}{\lambda} = \alpha + 2\epsilon \frac{\sin \theta}{\lambda} \tag{6}$$

$$\alpha = \frac{0.9}{D} \tag{7}$$

θ , λ , ϵ , and D are the diffraction angle, X-ray wavelength, strain, and average particle size, respectively. The dislocation density ρ , is derived by equation (8), as follows [36]:

$$\rho = 14.4 \frac{\epsilon^2}{b^2} \tag{8}$$

Here, b is the magnitude of the Burgers vector [37]. Table 2 shows the structure parameters of MgO, Mg_{0.99}Zn_{0.01}O, Mg_{0.97}Zn_{0.03}O nanoparticles.

Table 2
The structure parameters of MgO, Mg_{0.99}Zn_{0.01}O, Mg_{0.97}Zn_{0.03}O nanoparticles.

Compound	2θ±0.01	hkl	d _{hkl} (nm)±0.0005	Structure	Lattice parameter (nm) ±0.000005	V (Å ³)±0.000002	ε	cosφ	P (cm ⁻²) ±0.000005	Grain size (nm)
MgO	42.844	(200)	0.2109	Cubic	a = 0.421618	0.074947	0.014142	0.707107	1.017876	16
	62.225	(220)	0.1490							
Mg _{0.99} Zn _{0.01} O	31.8605	(200)	0.2109	Cubic	a = 0.421618	0.074947	0.015492	0.707107	1.017876	18
	34.5165	(220)	0.1490							
Mg _{0.97} Zn _{0.03} O	31.7625	(200)	0.2110	Cubic	a = 0.421859	0.075076	0.07746	0.707107	1.018458	13
	34.4273	(220)	0.1491							

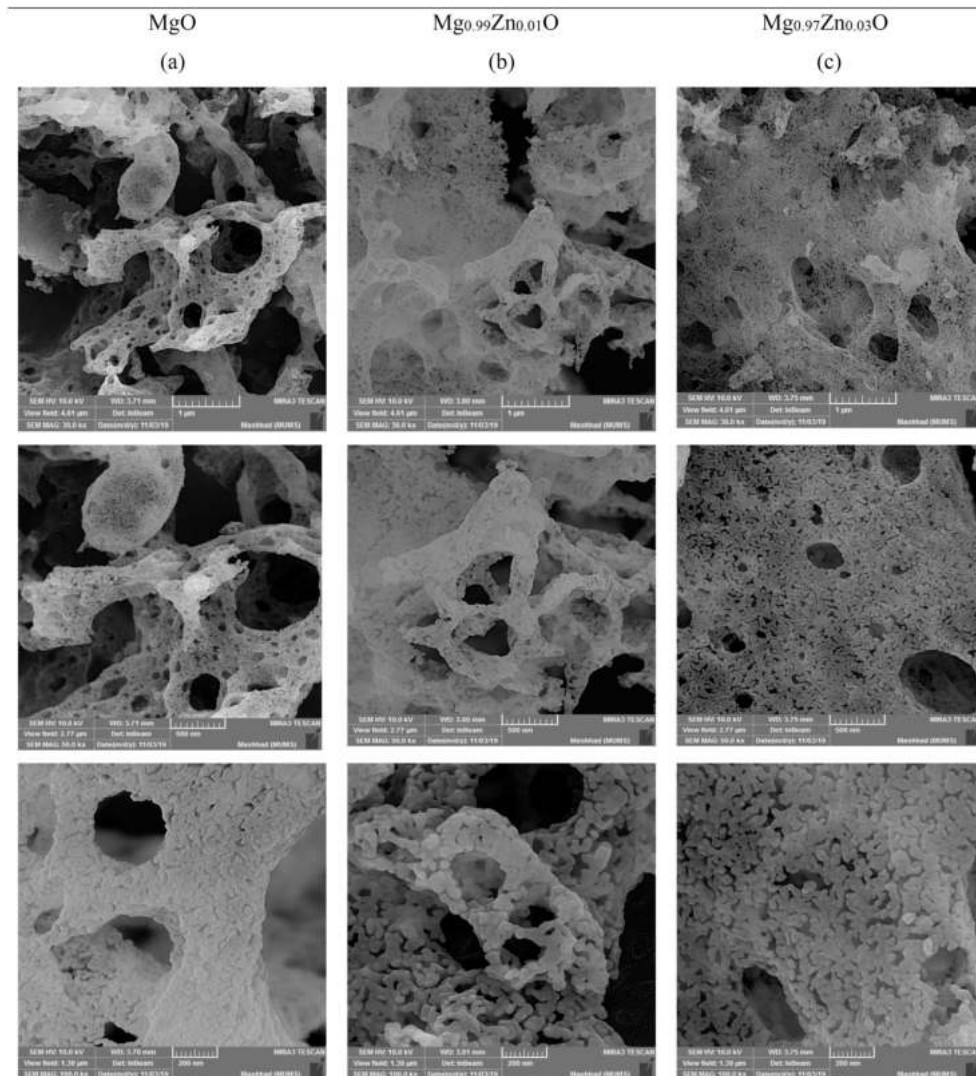


Fig. 4. FESEM images of (a) MgO(b) $Mg_{0.99}Zn_{0.01}O$, and (c) $Mg_{0.97}Zn_{0.03}O$ nanoparticles at magnification of 30 k, 50 k and 100 k respectively.

3.2. Nanoparticle and nanocomposite hydrogels microstructure

3.2.1. Nanoparticles microstructure

The FESEM microstructure images of $Mg_{0.97}Zn_{0.03}O$, $Mg_{0.99}Zn_{0.01}O$ and MgO nanoparticles are presented in Fig. 4. The high-resolution images of MgO powder showed the formation of nanoparticles, which were spherical in size, uniform, dense and porous with agglomeration. Loading the ZnO particles with MgO leads to form a hexagonal shape platelet [33]. The different properties of surface and various mechanisms of growth for $Mg_{0.99}Zn_{0.01}O$ and $Mg_{0.97}Zn_{0.03}O$ nanoparticles had affected by MgO. Additionally, by attaching the MgO to the ZnO, the suppression of crystal growth within the direction happened. Loading ZnO with MgO caused to grow a hexagonal structure independently. This phenomenon might be owing to the lower surface energy of a larger particle size; hence, the particles agglomeration did not happen to reduce the surface energy [38]. The formation of hexagonal platelet completed when loading with a high amount of MgO [39]. Thus, the doping of 'Zn' in MgO has a key impact on morphology and structural arrangement of MgO nanoparticles. The modification in morphological and structural properties of Zn-doped MgO nanoparticles take part in changing their thermal and optical properties [40]. In a study in 2015, Chen and his co-workers investigated the properties of MgZnO and BeMgZnO films that have been grown on c-plane sapphire substrates by plasma-assisted molecular beam epitaxy. They reported that MgZnO

film shows smooth surface with some small pits [41] that their findings were in agreement with findings of this research.

3.2.2. Nanocomposite hydrogels microstructure

The surface morphology of the $Mg_{0.99}Zn_{0.01}O$, $Mg_{0.97}Zn_{0.03}O$ and MgO nanocomposite is shown in Fig. 5. The rice-grain structure of MgO nanocomposite was observed by FESEM images. The rice-grain surface had a very smooth structure in the sample. Based on the FESEM images of $Mg_{0.99}Zn_{0.01}O$ and $Mg_{0.97}Zn_{0.03}O$ nanocomposite, a high amount of ZnO nanospheres gathered on the rice-grain structure surface. The porous structure of MgO, was the main reason to absorb the ZnO nanoparticles in the MgO rice-grain structure. Adsorption and penetration of the ions into the MgO during the preparation was supported by exposing of ZnO nanoparticles to the nanorice [42]. The FESEM images showed that Zn-doped MgO nanocomposites was more uniform than undoped nanoparticles (MgO nanoparticles) (Fig. 5(a-c)). The sizes of the ZnO samples did not significantly changed due to the incorporation of Mg atoms. As shown in Fig. 5, the shape of $x = 0.01$, and 0.03 MgZnO nanocomposites had no significant difference. Yaser Hossein studied the transparent conducting undoped and magnesium doped zinc oxide (MgZnO) thin films in a research in 2019. The $Mg_xZn_{1-x}O$ films grown with different Mg-doping content, and revealed that FESEM images of the morphological quality of ZnO films was found to be highly sensitive to the Mg content. It was observed that all the films possessed some

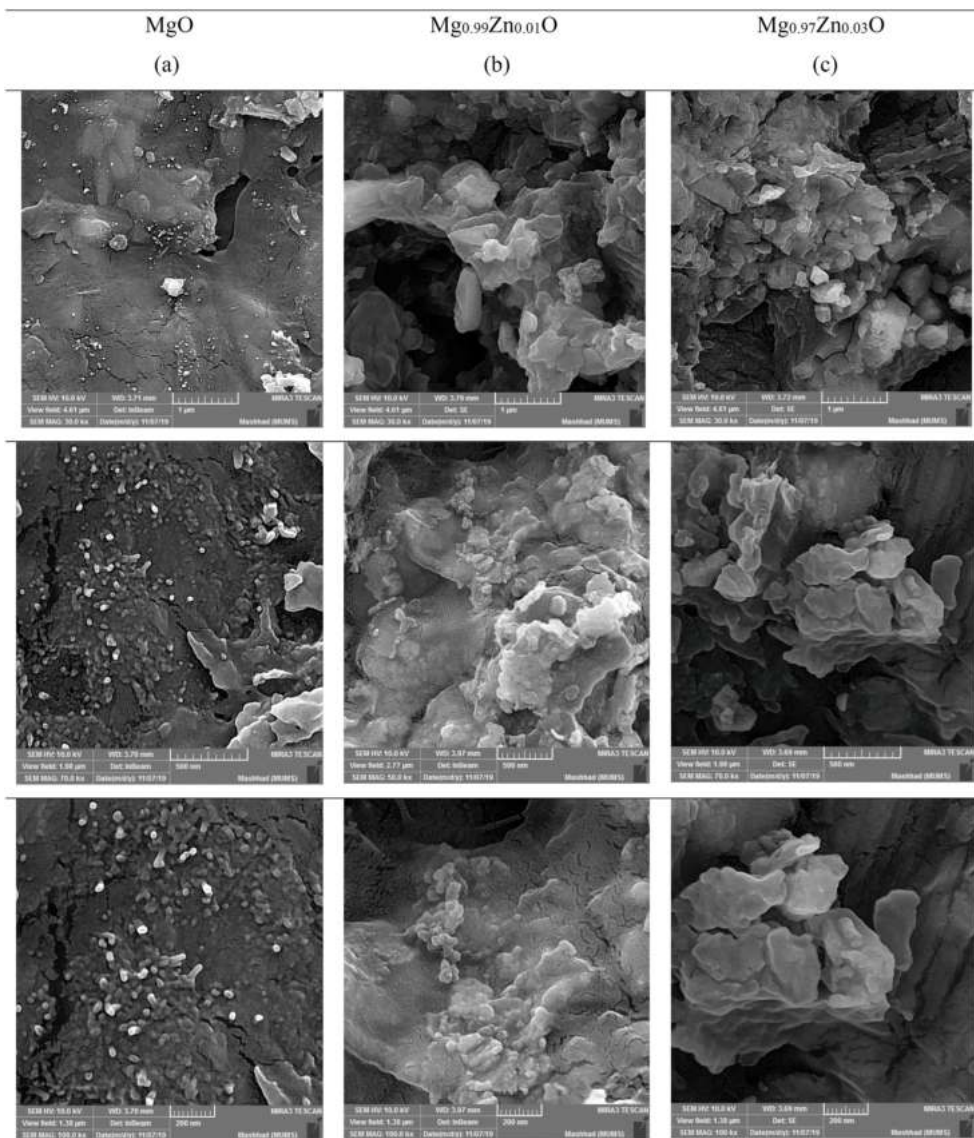


Fig. 5. FESEM images of (a) MgO(b) Mg_{0.99}Zn_{0.01}O, and (c) Mg_{0.97}Zn_{0.03}O nanocomposites at magnification of 30 k, 50 k and 100 k respectively.

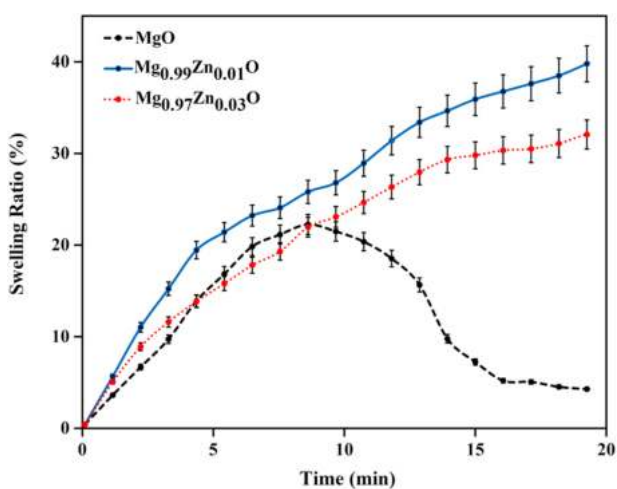


Fig. 6. Swelling capacity of MgO, Mg_{0.99}Zn_{0.01}O, and Mg_{0.97}Zn_{0.03}O nanocomposite hydrogels.

small grains wherein the sizes of these grains gradually minimized with the increase in the Mg level [43]. At higher percentage large particles are observed due to the agglomeration of the zinc oxide particles. This may be the reason for the decrease in mechanical properties at higher concentration [43]. In another study by Selvi et al., 2020, the micrographs of ZnO/MgO nanocomposites showed the formation of mushroom-like flakes. The different compositions reveal a small difference in the size and shape of particles. The findings of these researches were in agreement with this study [44].

3.3. Swelling ratio of nanocomposite hydrogels

The ability of hydrogels to swell in contact with a stable solvent or distilled water, is one of their most interesting properties. Determining the swelling characteristics of the system is important for relating its surface properties and mechanical properties of the composite system. The swelling equilibrium (maximum water uptake) is reached when the osmotic forces of the functional groups are balanced by the restrictive forces of the higher ordering of the polymer chains [7,45]. In Fig. 6, the swelling capability of Mg_{0.99}Zn_{0.01}O, and Mg_{0.97}Zn_{0.03}O nanocomposites hydrogel were compared to ZnO-free hydrogel (MgO nanocomposite). The swelling ratio of Mg_{0.99}Zn_{0.01}O started from

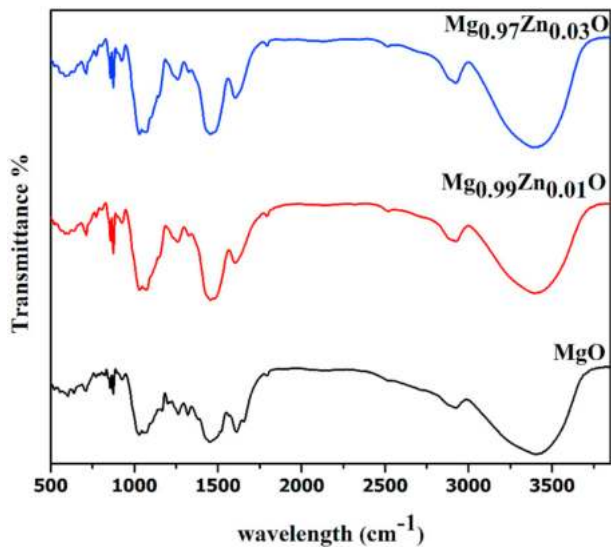


Fig. 7. FTIR spectra of MgO, Mg_{0.99}Zn_{0.01}O, and Mg_{0.97}Zn_{0.03}O nano-composite hydrogels.

5.51±2.61% and reached to 44.15±1.98% hence, the swelling ratio of Mg_{0.97}Zn_{0.03}O, started from 4.87±2.39% and reached to 35.38±0.87%. An increase in the content of zinc from 0.01 to 0.03 mg resulted decreasing the swelling ratio that due to the crosslinking act of ZnO nanoparticles [46]. While the content of cross-linker changes, the pore size would be changed that affecting the swelling ratio [47]. To obtain equilibrium osmosis pressure of this charge, more water molecules diffused into hydrogel nanocomposite that causes increase in swelling. The MgO nanocomposite had a swelling at 3.37±0.95% and reached to maximum water uptake at 3.81±0.26%. There was a peak at 22.1±6.76% in the graph which was related to starting of decrease in water absorption in the medium. This could be attributed to the weak stability of the composite rather than the Zn-incorporated nanocomposites. Fig. 6, also revealed that the pores in the structure of MgO nanocomposites were less than Mg_{0.99}Zn_{0.01}O and Mg_{0.97}Zn_{0.03}O nanocomposites that can be a cause of lesser swelling than the other two composites. Akbari et al. (2016), studied the influence of different amounts of ZnO nanoparticles on the swelling and drug release properties of bio nanocomposite hydrogels. Based on their results as compared to the pure hydrogel beads, the CMC/ZnO bio nanocomposite hydrogels showed a higher swelling degree and the increasing of the swelling degree of the CMC/ZnO bio nanocomposite hydrogels may be originated from the presence of ZnO nanoparticles with different sizes, morphologies and surface charges. In another study by Sabbagh et al., 2020, the swelling rate of κ -Carrageenan/Mg_{0.99}Zn_{0.01}O/NaCMC was higher than κ -Carrageenan/NaCMC. These results are in agreement with the findings of this research [48].

3.4. FTIR chemical characterization

Fig. 7 shows the FTIR spectrum of Mg_{0.99}Zn_{0.01}O, Mg_{0.97}Zn_{0.03}O and MgO powder nanocomposite in the frequency range (400–4000 cm⁻¹). For MgO, the peak in the range of 540–570 cm⁻¹ was related to C–C skeleton vibration, which in the MgO spectrum was at 551.19 cm⁻¹, but in Mg_{0.99}Zn_{0.01}O, and Mg_{0.97}Zn_{0.03}O spectra were shifted to 552.59 cm⁻¹. The peaks from 455 to 670 cm⁻¹ showed the skeletal vibration, this peak was at 601.47 cm⁻¹ in the MgO graph and shifted to 586.75 cm⁻¹ at Mg_{0.99}Zn_{0.01}O and at 586.22 cm⁻¹ at Mg_{0.97}Zn_{0.03}O graph. The peak at 426.0 cm⁻¹ indicated Mg–O bond stretching, which in turn confirmed that the obtained product was magnesium oxide, and around 450 cm⁻¹ Zn–O stretching found in the IR spectrum of ZnO nanoparticles. The peaks from 500 to 730 cm⁻¹ perform the symmetrically

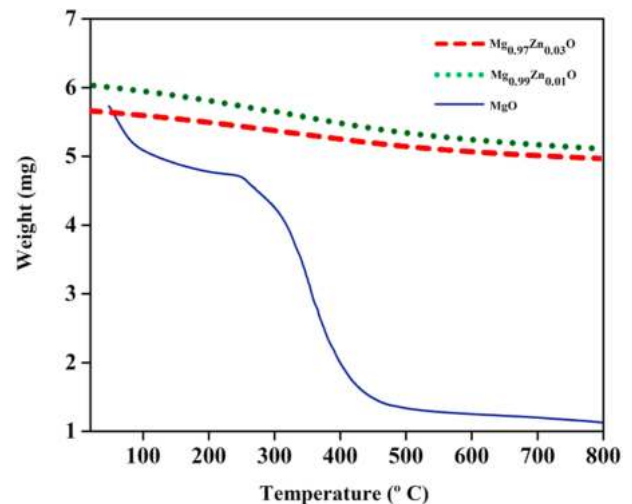


Fig. 8. TGA curves of MgO, Mg_{0.99}Zn_{0.01}O, and Mg_{0.97}Zn_{0.03}O nano-composite hydrogels.

stretching vibration. In the MgO graph, this peak is at 641.09 cm⁻¹, in Mg_{0.99}Zn_{0.01}O nanocomposite, the mentioned peak is shifted to 712.08 cm⁻¹ and in Mg_{0.97}Zn_{0.03}O nanocomposite it is at 711.29 cm⁻¹. The peaks from 835 cm⁻¹ to 865 cm⁻¹ presented the S–H bending vibration. In the MgO nanocomposite graph, this peak presented at 855.18 cm⁻¹ and shifted to 856.08 cm⁻¹ in Mg_{0.99}Zn_{0.01}O and Mg_{0.97}Zn_{0.03}O nanocomposite. 870–900 cm⁻¹ corresponds for CH₃–metal groups due to CH₂ rocking vibration. The peak at 926 cm⁻¹ in the MgO graph showed the CH₃ rocking vibration. In the nanocomposite graphs, C–H rocking vibration presented at 1028–1030 cm⁻¹. C–O stretching vibration confirmed by 1061–1085 cm⁻¹. This peak was 1061.97 cm⁻¹ at the MgO graph which shifted to 1078.32 cm⁻¹ in Mg_{0.99}Zn_{0.01}O and 1070.15 cm⁻¹ in Mg_{0.97}Zn_{0.03}O nanocomposites. The peaks 1064–1320 cm⁻¹ show the various bands in cellulose. The presence of cellulose in all three nanocomposites is confirmed at peak number 1064.13 cm⁻¹ in MgO nanocomposite, 1078.32 cm⁻¹ in Mg_{0.99}Zn_{0.01}O, and 1147.79 cm⁻¹ in Mg_{0.97}Zn_{0.03}O nanocomposites. The C–H deformation vibration at 1375 cm⁻¹ was related to cellulose and at 1380 cm⁻¹ was related to O–H deformation vibration. Peak at 1410–1495 cm⁻¹ confirmed the presence of CaCO₃ in polymer additives. Meanwhile, the asymmetric CO₂⁻ stretching vibration shown by 1550–1650 cm⁻¹ bonds. 1710–1810 cm⁻¹ presents the C=O stretching vibration. 2340–2790 cm⁻¹ was related to primary alcoholic O–H functional group and O–H stretching vibration in the structure of carrageenan. The peaks from 2920 to 2950 cm⁻¹ shows the asymmetrically CH₂ stretching vibration. The peak at 3410 cm⁻¹ in MgO nanocomposite graph, the peak at 3398 cm⁻¹ in Mg_{0.99}Zn_{0.01}O nanocomposites and 3389 cm⁻¹ in Mg_{0.97}Zn_{0.03}O nanocomposites was related to O–H stretching vibration which confirmed at 3125–3575 cm⁻¹. This information is in agreement with the research of Pachiyappan et al., 2020 [49]. They prepared ZnO, ZnO–MgO nanocomposites (NC-1, NC-2, NC-3) and MgO nanocomposite materials. They showed that the broad spectrum around 3492 cm⁻¹, 2945 cm⁻¹, 1752 cm⁻¹, 1487 cm⁻¹, 1287 cm⁻¹, 843 cm⁻¹ and 562 cm⁻¹ were also detected in their study.

3.5. TGA characterization

To consider the impact of concentration of doping on thermal properties of Zn-doped MgO and pure nanoparticles, thermogravimetric analysis (TGA) was carried out. Fig. 8 shows the thermal behavior of decomposition of MgO, Mg_{0.99}Zn_{0.01}O, and Mg_{0.97}Zn_{0.03}O nanocomposites. For all polymer systems, the first degradation process that starts below 100°C which attributed to the loss of bound water [50]. The weight loss occurring below 380 °C, is owing to the evaporation of

Table 3
Compression test of the MgO, Mg_{0.99}Zn_{0.01}O, and Mg_{0.97}Zn_{0.03}O nanocomposite hydrogels.

Sample	Hardness (g)	Springiness (mm)	Adhesion (g.s)	Consistency (g. sec)
MgO nanocomposite	84.75±9.19	8	-1.195±0.46	330.22±7.10
Mg _{0.99} Zn _{0.01} O nanocomposite	77.85±3.40	10	-0.848±0.17	392.90±3.48
Mg _{0.97} Zn _{0.03} O nanocomposite	80.43±2.64	10	-0.848±0.29	376.20±0.29

organic compounds and water and dihydroxylation of hydroxide precursor to oxide compound [51–53]. The second weight loss between 380 °C and 430 °C with an endothermic peak at 430 °C was attributed to the nitrate group decomposition and the third weight loss between 430 °C and 800 °C was due to the complete decomposition of precursor to MgO and also ZnO in Mg_{0.99}Zn_{0.01}O, and Mg_{0.97}Zn_{0.03}O nanocomposites. A comparison of curves in Fig. 8 shows that total weight loss of pure MgO was more than Mg_{0.99}Zn_{0.01}O, and Mg_{0.97}Zn_{0.03}O whereas, the decomposition temperature of pure MgO (380 °C–800 °C) was higher than the Mg_{0.99}Zn_{0.01}O, and Mg_{0.97}Zn_{0.03}O (75–800 °C). It displays that the phase transition decreases because of the weight loss reduction as a result of doping of 'Mg' in ZnO and the composites become more steady [40]. This study is in agreement with the research of Parvizi et al., 2019 [54]. They synthesized MgZnO@SiO₂-tetrazine nanoparticles. The first gradual and continuous weight-loss occurred below 200 °C, which was most likely due to water desorption from the surface of particles and loss of moisture content. Further loss at higher temperatures was probably corresponded to the progressive burning of the alkyl remnants which was accompanied with the crystallization of zinc oxide up to 530 °C.

3.6. Compression test: mechanical characterization

The results of the compression test (hardness, springiness, adhesion, and consistency) of the nanocomposite hydrogels are presented in Table 2. The hardness of MgO nanocomposite was 84.75±9.19 (g) which was higher than that of Mg_{0.97}Zn_{0.03}O and Mg_{0.99}Zn_{0.01}O nanocomposites: (Hardness: MgO > Mg_{0.97}Zn_{0.03}O > Mg_{0.99}Zn_{0.01}O). The consequences of springiness revealed that Mg_{0.97}Zn_{0.03}O and Mg_{0.99}Zn_{0.01}O nanocomposites were the same as 10 mm, but MgO nanocomposite showed the lesser springiness than the other samples; therefore, (Springiness: Mg_{0.97}Zn_{0.03}O and Mg_{0.99}Zn_{0.01}O > MgO). The adhesion and consistency of Mg_{0.99}Zn_{0.01}O are -0.848±0.17 (g. s) and 392.90±19.48 (g. sec) that was higher than Mg_{0.97}Zn_{0.03}O and MgO nanocomposites (p > 0.05). Therefore, it concluded from Table 3, that (Adhesion: Mg_{0.99}Zn_{0.01}O > Mg_{0.97}Zn_{0.03}O > MgO) and (Consistency: Mg_{0.99}Zn_{0.01}O > Mg_{0.97}Zn_{0.03}O > MgO).

The interface interaction between a polymer matrix and the interface interaction caused to increase in properties which is valuable for development of the composite films' tensile strength. However aggregation occurs owing to the increasing content of nanoparticles, that causes to a reduction in the contact area between the polymer matrix and the nanoparticles, so the results defects in the composites. Hence, the tensile strength of the films gets decreased due to the reduction of the applicable interfacial interaction. The nanoparticles dispersion through the matrix is also affected by the mechanical properties. These results are in line with the findings of Sabbagh et al., 2020 [30]. They produced a κ-Carrageenan/Mg_{0.99}Zn_{0.01}O/NaCMC hydrogel based on the green synthesis of nanoparticles. They found that the covalent compositing of κ-Carrageenan/NaCMC hydrogels with Mg_{0.99}Zn_{0.01}O nanoparticles achieved higher mechanical strength rather than the nanoparticle-free hydrogel. The covalent compositing with particles increases the hardness and adhesion of the samples.

4. Conclusion

The XRD results showed that the intense and sharp peaks in the MgO cubic structure and ZnO hexagonal were highly crystalline. The FESEM

analysis revealed that surface features of the spherical size with uniform size of MgO nanoparticles are strongly dependent on the doping concentration of 'Zn'. The swelling ratio of Mg_{0.99}Zn_{0.01}O, was higher than Mg_{0.97}Zn_{0.03}O and MgO hydrogels due to the strong stability of the Zn-incorporated composite rather than MgO nanocomposites. The FTIR curve confirmed that the doping of Zn and MgO has occurred properly and the effect of doped nanoparticles is obvious in the curves. Thermogravimetry analysis showed that the thermal stability of MgO increased after doping with 'Zn'. The compression test showed that MgO nanocomposites had a stronger structure. Besides, the comparison between the Zn-doped samples showed more Zn content due to the higher stability and hardness of the resultant nanocomposite hydrogels. The results indicated that Zn-doped MgO nanoparticles are an efficient candidate for drug delivery applications.

CRediT authorship contribution statement

Farzaneh Sabbagh: Conceptualization, Methodology, Data curation, Writing - original draft, preparation. **Khadijeh Kiarostami:** Visualization, Investigation, Supervision. **Nadia Mahmoudi Khatir:** Software, Validation. **Shahabaldin Rezaia:** Writing - review & editing, Formal analysis. **Ida Idayu Muhamad:** Project administration, Resources. **Fakhrisadat Hosseini:** Writing - review & editing.

Declaration of competing interest

The authors declare that they have no known competing financial interests or personal relationships that could have appeared to influence the work reported in this paper.

Acknowledgements

We acknowledge the technical support of Alzahra university.

Appendix A. Supplementary data

Supplementary data to this article can be found online at <https://doi.org/10.1016/j.polymertesting.2020.106922>.

References

- [1] K. Shalumon, K. Anulekha, S.V. Nair, S. Nair, K. Chennazhi, R. Jayakumar, Sodium alginate/poly (vinyl alcohol)/nano ZnO composite nanofibers for antibacterial wound dressings, *Int. J. Biol. Macromol.* 49 (2011) 247–254.
- [2] N. Alipoormazandarani, S. Ghazihoseini, A.M. Nafchi, Preparation and characterization of novel bionanocomposite based on soluble soybean polysaccharide and halloysite nanoclay, *Carbohydr. Polym.* 134 (2015) 745–751.
- [3] M.T. Khorasani, A. Joorabloo, A. Moghaddam, H. Shamsi, Z. Mansoori Moghadam, Incorporation of ZnO nanoparticles into heparinised poly(vinyl alcohol)/chitosan hydrogels for wound dressing application, *Int. J. Biol. Macromol.* 114 (2018) 1203–1215.
- [4] S. Aksoy, Y. Caglar, S. Ilican, M. Caglar, Sol-gel derived Li-Mg co-doped ZnO films: preparation and characterization via XRD, XPS, FESEM, *J. Alloys Compd.* 512 (2012) 171–178.
- [5] B. González-Penguely, Á. de Jesús Morales-Ramírez, M.G. Rodríguez-Rosales, C. O. Rodríguez-Nava, M.L. Carrera-Jota, New infrared-assisted method for sol-gel derived ZnO: Ag thin films: structural and bacterial inhibition properties, *Mater. Sci. Eng. C* 78 (2017) 833–841.
- [6] R. Dadi, R. Azouani, M. Traore, C. Mielcarek, A. Kanaev, Antibacterial activity of ZnO and CuO nanoparticles against gram positive and gram negative strains, *Mater. Sci. Eng. C* 104 (2019) 109968.
- [7] N.M. El-Sawy, A.I. Raafat, N.A. Badawy, A.M. Mohamed, Radiation development of pH-responsive (xanthan-acrylic acid)/MgO nanocomposite hydrogels for

- controlled delivery of methotrexate anticancer drug, *Int. J. Biol. Macromol.* 142 (2020) 254–264.
- [8] S.V. Sudakaran, J.R. Venugopal, G.P. Vijayakumar, S. Abisegapriyan, A.N. Grace, S. Ramakrishna, Sequel of MgO nanoparticles in PLACL nanofibers for anti-cancer therapy in synergy with curcumin/ β -cyclodextrin, *Mater. Sci. Eng. C* 71 (2017) 620–628.
- [9] F. Sabbagh, I.I. Muhamad, Z. Nazari, P. Mobini, S.B. Tarahdari, From formulation of acrylamide-based hydrogels to their optimization for drug release using response surface methodology, *Mater. Sci. Eng. C* 92 (2018) 20–25.
- [10] F. Sabbagh, N.M. Khatir, A.K. Karim, A. Omidvar, Z. Nazari, R. Jaber, Mechanical properties and swelling behavior of acrylamide hydrogels using mont-morillonite and kaolinite as clays, *Journal of Environmental Treatment Techniques* 7 (2019) 211–219.
- [11] L. Li, J. Zhao, Y. Sun, F. Yu, J. Ma, Ionically cross-linked sodium alginate/ κ -carrageenan double-network gel beads with low-swelling, enhanced mechanical properties, and excellent adsorption performance, *Chem. Eng. J.* 372 (2019) 1091–1103.
- [12] A.O. Kravchenko, S.D. Anastuyk, V.P. Glazunov, E.V. Sokolova, V.V. Isakov, I. M. Yermak, Structural characteristics of carrageenans of red alga *Mastocarpus pacificus* from sea of Japan, *Carbohydr. Polym.* 229 (2020) 115518.
- [13] A.I. Usov, Polysaccharides of the red algae, *Advances in Carbohydrate Chemistry and Biochemistry*, Elsevier, 2011, pp. 115–217.
- [14] G.R. Mahdavinia, Z. Rahmani, S. Karami, A. Pourjavadi, Magnetic/pH-sensitive κ -carrageenan/sodium alginate hydrogel nanocomposite beads: preparation, swelling behavior, and drug delivery, *J. Biomater. Sci. Polym. Ed.* 25 (2014) 1891–1906.
- [15] I. Priyan Shanura Fernando, K.-N. Kim, D. Kim, Y.-J. Jeon, Algal polysaccharides: potential bioactive substances for cosmeceutical applications, *Crit. Rev. Biotechnol.* 39 (2019) 99–113.
- [16] V.A. Cosenza, D.A. Navarro, N.M. Ponce, C.A. Stortz, *Seaweed Polysaccharides: Structure and Applications, Industrial Applications of Renewable Biomass Products*, Springer, 2017, pp. 75–116.
- [17] F. Sabbagh, I.I. Muhamad, Physical and chemical characterisation of acrylamide-based hydrogels, Aam, Aam/NaCMC and Aam/NaCMC/MgO, *J. Inorg. Organomet. Polym. Mater.* 27 (2017) 1439–1449.
- [18] H. Yuan, J. Song, X. Li, N. Li, S. Liu, Enhanced immunostimulatory and antitumor activity of different derivatives of κ -carrageenan oligosaccharides from *Kappaphycus striatum*, *J. Appl. Phycol.* 23 (2011) 59–65.
- [19] S. Tavakoli, H. Mokhtari, M. Kharaziha, A. Kermanpour, A. Talebi, J. Moshaghian, A multifunctional nanocomposite spray dressing of Kappa-carrageenan-polydopamine modified ZnO/L-glutamic acid for diabetic wounds, *Mater. Sci. Eng. C* (2020) 110837.
- [20] E. Sokolova, L. Bogdanovich, T. Ivanova, A. Byankina, S. Kryzhanovskiy, I. Yermak, Effect of carrageenan food supplement on patients with cardiovascular disease results in normalization of lipid profile and moderate modulation of immunity system markers, *PharmaNutrition* 2 (2014) 33–37.
- [21] S.G. Jin, K.S. Kim, D.W. Kim, D.S. Kim, Y.G. Seo, T.G. Go, Y.S. Youn, J.O. Kim, C. S. Yong, H.-G. Choi, Development of a novel sodium fusidate-loaded triple polymer hydrogel wound dressing: mechanical properties and effects on wound repair, *Int. J. Pharm.* 497 (2016) 114–122.
- [22] N.M. Khatir, Z. Abdul-Malek, A.K. Zak, A. Akbari, F. Sabbagh, Sol-gel grown Fe-doped ZnO nanoparticles: antibacterial and structural behaviors, *J. Sol. Gel Sci. Technol.* 78 (2016) 91–98.
- [23] L. Duque, M. Körber, R. Bodmeier, Impact of change of matrix crystallinity and polymorphism on ovalbumin release from lipid-based implants, *Eur. J. Pharmaceut. Sci.* 117 (2018) 128–137.
- [24] Z. Haghparasti, M.M. Shahri, Green synthesis of water-soluble nontoxic inorganic polymer nanocomposites containing silver nanoparticles using white tea extract and assessment of their in vitro antioxidant and cytotoxicity activities, *Mater. Sci. Eng. C* 87 (2018) 139–148.
- [25] A. Turlybekuly, A. Pogrebnyak, L. Sukhodub, L.B. Sukhodub, A. Kistaubayeva, I. Savitskaya, D. Shokatayeva, O.V. Bondar, Z.K. Shaimardanov, S.V. Plotnikov, Synthesis, characterization, in vitro biocompatibility and antibacterial properties study of nanocomposite materials based on hydroxyapatite-biphasic ZnO micro- and nanoparticles embedded in Alginate matrix, *Mater. Sci. Eng. C* 104 (2019) 109965.
- [26] F. Sabbagh, I.I. Muhamad, Z. Nazari, P. Mobini, N.M. Khatir, Investigation of acyclovir-loaded, acrylamide-based hydrogels for potential use as vaginal ring, *Materials Today Communications* 16 (2018) 274–280.
- [27] G. Manasa, R.J. Mascarenhas, A.K. Satpati, O.J. D'Souza, A. Dhason, Facile preparation of poly (methylene blue) modified carbon paste electrode for the detection and quantification of catechin, *Mater. Sci. Eng. C* 73 (2017) 552–561.
- [28] E. Zohourvahid-Karimi, A. Moloodi, J.V. Khaki, A study on carbon nanotubes/nanofibers production via SHS method in C-Al-Fe₂O₃ system, *Journal of Materials Research and Technology* 7 (2018) 212–217.
- [29] J. Chen, W. Chen, F. Duan, Q. Tang, X. Li, L. Zeng, J. Zhang, Z. Xing, Y. Dong, L. Jia, The synergistic gelation of okra polysaccharides with kappa-carrageenan and its influence on gel rheology, texture behaviour and microstructures, *Food Hydrocolloids* 87 (2019) 425–435.
- [30] F. Sabbagh, K. Kiarostami, N. Mahmoudi Khatir, S. Rezania, I.I. Muhamad, Green synthesis of MgO. 99 ZnO. 010 nanoparticles for the fabrication of κ -carrageenan/NaCMC hydrogel in order to deliver catechin, *Polymers* 12 (2020) 861.
- [31] S. Zhang, Y. Zhao, C. Ohland, C. Jobin, S. Sang, Microbiota facilitates the formation of the aminated metabolite of green tea polyphenol (-)-epigallocatechin-3-gallate which trap deleterious reactive endogenous metabolites, *Free Radic. Biol. Med.* 131 (2019) 332–344.
- [32] Y. Liu, Y. Qin, R. Bai, X. Zhang, L. Yuan, J. Liu, Preparation of pH-sensitive and antioxidant packaging films based on κ -carrageenan and mulberry polyphenolic extract, *Int. J. Biol. Macromol.* 134 (2019) 993–1001.
- [33] G. Balakrishnan, R. Velavan, K.M. Batoo, E.H. Raslan, Microstructure, optical and photocatalytic properties of MgO nanoparticles, *Results in Physics* 16 (2020) 103013.
- [34] <http://duffy.princeton.edu/sites/default/files/pdfs/links/xtalgeometry.pdf>.
- [35] G. Williamson, W. Hall, X-ray line broadening from filed aluminium and wolfram, *Acta Metall.* 1 (1953) 22–31.
- [36] G. Williamson, R. Smallman III., Dislocation densities in some annealed and cold-worked metals from measurements on the X-ray debye-scherrer spectrum, *Phil. Mag.* 1 (1956) 34–46.
- [37] S. Takebayashi, T. Kunieda, N. Yoshinaga, K. Ushioda, S. Ogata, Comparison of the dislocation density in martensitic steels evaluated by some X-ray diffraction methods, *ISIJ Int.* 50 (2010) 875–882.
- [38] S. Klubnuan, P. Amornpitoksuk, S. Suwanboon, Structural, optical and photocatalytic properties of MgO/ZnO nanocomposites prepared by a hydrothermal method, *Mater. Sci. Semicond. Process.* 39 (2015) 515–520.
- [39] L. Cavalcante, N. Batista, T. Badapanda, M. Costa, M. Li, W. Avansi, V.R. Mastelaro, E. Longo, J. Espinosa, M. Gurgel, Local electronic structure, optical bandgap and photoluminescence (PL) properties of Ba (ZrO. 75TiO. 25) O₃ powders, *Mater. Sci. Semicond. Process.* 16 (2013) 1035–1045.
- [40] R. Sagheer, M. Khalil, V. Abbas, Z.N. Kayani, U. Tariq, F. Ashraf, Effect of Mg doping on structural, morphological, optical and thermal properties of ZnO nanoparticles, *Optik* 200 (2020) 163428.
- [41] S. Chen, X. Pan, Y. Li, W. Chen, H. Zhang, W. Dai, P. Ding, J. Huang, B. Lu, Z. Ye, Improved photoluminescence performance of MgZnO films by alloying beryllium, *Phys. Lett.* 379 (2015) 912–915.
- [42] Y.H. Mohammed, Fabrication of n-MgZnO/p-Si heterojunction diode: role of magnesium doping, *Superlattice. Microsc.* 131 (2019) 104–116.
- [43] S.K. Esthappan, A.B. Nair, R. Joseph, Effect of crystallite size of zinc oxide on the mechanical, thermal and flow properties of polypropylene/zinc oxide nanocomposites, *Compos. B Eng.* 69 (2015) 145–153.
- [44] K.T. Selvi, K.A. Mangai, M. Priya, S. Sagadevan, Investigation of the dielectric and impedance properties of ZnO/MgO nanocomposite, *Phys. B Condens. Matter* (2020) 412355.
- [45] H. Namazi, M. Hasani, M. Yadollahi, Antibacterial oxidized starch/ZnO nanocomposite hydrogel: synthesis and evaluation of its swelling behaviours in various pHs and salt solutions, *Int. J. Biol. Macromol.* 126 (2019) 578–584.
- [46] Ž. Jovanović, A. Krklješ, J. Stojkowska, S. Tomić, B. Obradović, V. Mišković-Stanković, Z. Kačarević-Popović, Synthesis and characterization of silver/poly (N-vinyl-2-pyrrolidone) hydrogel nanocomposite obtained by in situ radiolytic method, *Radiat. Phys. Chem.* 80 (2011) 1208–1215.
- [47] F. Sabbagh, I.I. Muhamad, Acrylamide-based hydrogel drug delivery systems: release of acyclovir from MgO nanocomposite hydrogel, *Journal of the Taiwan Institute of Chemical Engineers* 72 (2017) 182–193.
- [48] Z. Zare-Akbari, H. Farhadnejad, B. Furughi-Nia, S. Abedin, M. Yadollahi, M. Khorsand-Ghayeni, PH-sensitive bionanocomposite hydrogel beads based on carboxymethyl cellulose/ZnO nanoparticle as drug carrier, *Int. J. Biol. Macromol.* 93 (2016) 1317–1327.
- [49] J. Pachiyappan, N. Gnanasundaram, G.L. Rao, Preparation and characterization of ZnO, MgO and ZnO-MgO hybrid nanomaterials using green chemistry approach, *Results in Materials* (2020) 100104.
- [50] A.G. Rusu, M.I. Popa, G. Lisa, L. Vereștiuc, Thermal behavior of hydrophobically modified hydrogels using TGA/FTIR/MS analysis technique, *Thermochim. Acta* 613 (2015) 28–40.
- [51] H.B. Dias, M.I.B. Bernardi, V.S. Marangoni, A.C. de Abreu Bernardi, A.N. de Souza Rastelli, A.C. Hernandez, Synthesis, characterization and application of Ag doped ZnO nanoparticles in a composite resin, *Mater. Sci. Eng. C* 96 (2019) 391–401.
- [52] A. Phruangrat, T. Thongtem, S. Thongtem, Synthesis, characterization and ferromagnetic properties of Zn_{1-x}Mn_xO ($x \leq 0.05$) nanoparticles, *J. Mol. Struct.* 1161 (2018) 108–112.
- [53] D. Raoufi, Synthesis and microstructural properties of ZnO nanoparticles prepared by precipitation method, *Renew. Energy* 50 (2013) 932–937.
- [54] E. Parvizi, R. Tayebee, E. Koushki, M.F. Abdzadeh, B. Maleki, P. Audebert, L. Galmiche, Photocatalytic efficacy of supported tetrazine on MgZnO nanoparticles for the heterogeneous photodegradation of methylene blue and ciprofloxacin, *RSC Adv.* 9 (2019) 23818–23831.